J. Fluid Mech. (2004), *vol.* 501, *pp.* 231–250.
DOI: 10.1017/S0022112003007572 Printed in the United Kingdom

Steady nonlinear waves in diverging channel flow

By R. R. KERSWELL[1], O. R. TUTTY[2] AND P. G. DRAZIN[1]†

[1]Department of Mathematics, Bristol University, Bristol BS8 1TW, UK

[2]School of Engineering Sciences, Southampton University, Southampton SO17 1BJ, UK

(Received 15 May 2003 and in revised form 5 September 2003)

An infinitely diverging channel with a line source of fluid at its vertex is a natural idealization of flow in a finite channel expansion. Motivated by numerical results obtained in an associated geometry (Tutty 1996), we show in this theoretical model that for certain channel semi-angles α and Reynolds numbers $Re := Q/2\nu$ (Q is the volume flux per unit length and ν the kinematic viscosity) a steady, spatially periodic, two-dimensional wave exists which appears spatially stable and hence plausibly realizable in the physical system. This spatial wave (or limit cycle) is born out of a heteroclinic bifurcation across the subcritical pitchfork arms which originate out of the well known Jeffery–Hamel bifurcation point at $\alpha = \alpha_2(Re)$. These waves have been found over the range $5 \leqslant Re \leqslant 5000$ and, significantly, exist for semi-angles α beyond the point α_2 where Jeffery–Hamel theory has been shown to be mute. However, the limit of $\alpha \to 0$ at finite Re is not reached and so these waves have no relevance to plane Poiseuille flow.

1. Introduction

Tutty (1996) has computed the solutions for some two-dimensional steady flows of an incompressible viscous fluid along channels with long sections in which the walls are plane and inclined at quite small angles. Although the channels have quite complicated inlet and outlet regions, the long sections approximate well the ideal conditions assumed by Jeffery and Hamel in deriving their exact solutions of the Navier–Stokes equations for unbounded flow between inclined rigid planes (see, e.g., Batchelor 1967, § 5.6). Some of Tutty's solutions (Tutty 1996, figures 7, 9) are remarkable because they are, as nearly as the eye can see, periodic downstream in the variable

$$\rho := \log r_*,$$

where r_* is the radial coordinate such that the line of intersection of the extended plane channel walls is $r_* = 0$. These numerical solutions suggest that there exist hitherto unknown periodic nonlinear steady wave solutions of the Jeffery–Hamel configuration. Tutty's waves seem to be symmetric, whereby they are invariant if translated half a wavelength and reflected in the centre plane between the two inclined plane walls. The ready convergence of Tutty's iteration of his numerical procedure suggests plausibly that the periodic solutions may be stable.

These results invite a systematic investigation of the existence and properties of exactly periodic nonlinear steady wave solutions of the Jeffery–Hamel configuration. To explain this, it is helpful first to recapitulate the relevant results for the

† Professor Drazin died on 10 January 2002.

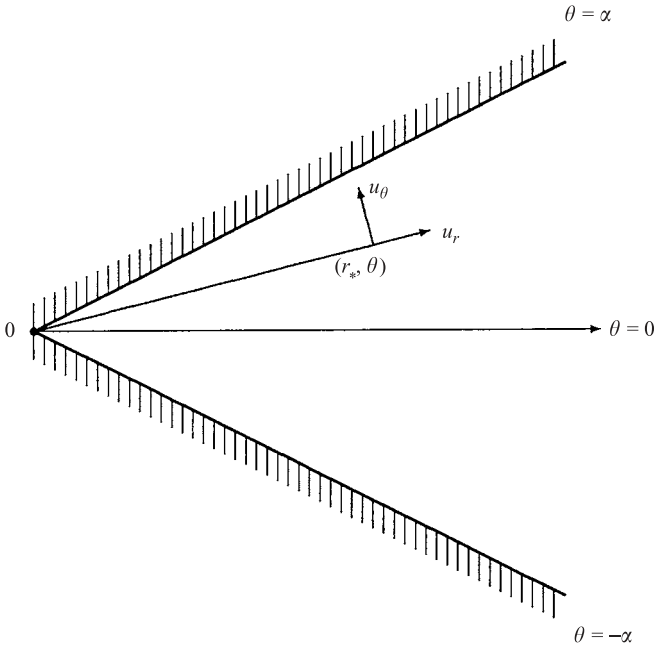

FIGURE 1. Configuration and notation of Jeffery–Hamel flows.

classic Jeffery–Hamel problem. Consider then the steady two-dimensional flow of an incompressible viscous fluid between two inclined rigid planes $\theta = \pm\alpha$ driven by a line source at $r_* = 0$ of volume flux Q per unit length. Here plane polar coordinates r_*, θ are used, and the configuration of the flows is shown in figure 1. It is convenient to define the Reynolds number as

$$Re := Q/2\nu, \tag{1}$$

where ν is the kinematic viscosity of the fluid. The classic theory of Jeffery and Hamel (see Fraenkel 1962 for a definitive account) treats similarity solutions by assuming purely radial flow, such that the streamfunction $\psi_* = \Psi_*(\theta)$ and the radial velocity $u_r = r_*^{-1}\Psi_*'(\theta)$. It is found that for each given pair of dimensionless parameters α, Re there is an infinity of Jeffery–Hamel flows (Fraenkel 1962), but that only the unique solution with unidirectional flow, when it exists, is spatially stable (Banks, Drazin & Zaturska 1988). In this paper we adopt the nomenclature of Fraenkel (1962) and consider only divergent channel flow. The unique spatially stable unidirectional divergent flow (i.e. pure outflow) is therefore referred to as II_1. This is a flow symmetric about the channel's midplane, that is $u_r(-\theta) = u_r(\theta)$. Flow II_1 is known to become spatially unstable (Sobey & Drazin 1986) through a subcritical pitchfork bifurcation (see figure 2) as the semi-angle α increases through $\alpha_2(Re)$ ($\alpha_2(0) = \frac{1}{2}\pi$ and $\alpha_2(Re) \sim 4.712/Re$ as $Re \to \infty$). The spatially unstable symmetric flow for $\alpha > \alpha_2$ is known as type II_2 and the spatially unstable asymmetric states are labelled as types IV_1 and V_1 (see figure 2) where V_1 is the mirror image of IV_1 in the channel midplane. Since just trivial state II_1 is predicted to be spatially stable, the study of Jeffery–Hamel flows makes only the modest prediction of the realizable flow for $\alpha < \alpha_2(Re)$. The II_1 solution is predicted to lose stability through a *sub*critical pitchfork bifurcation. There are no numerical or experimental studies with which to make a direct comparison of this prediction. Those studies that do exist on flow in expanding channels have

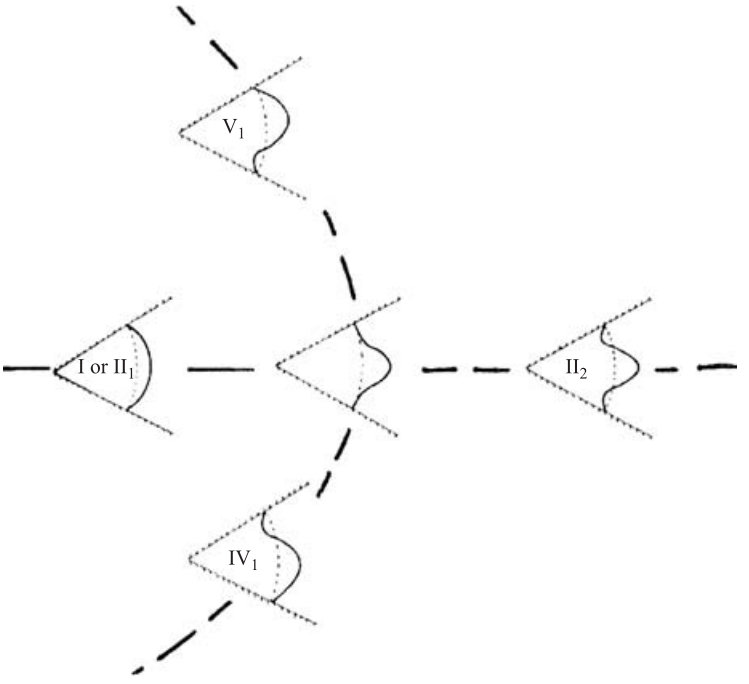

FIGURE 2. Velocity profiles of the more-important Jeffery–Hamel flows and a symbolic indication of their subcritical pitchfork bifurcation.

sudden (step) or finite expansions. However, in all such studies, either experimental (Cherdron, Durst & Whitelaw 1978; Nakayama 1988; Sobey & Drazin 1986) or numerical (Cliffe & Greenfield 1982; Sobey & Drazin 1986; Fearn, Mullin & Cliffe 1990; Alleborn *et al.* 1997), a *super*critical pitchfork is invariably found. Therefore the contact Jeffery–Hamel flow theory in an infinitely diverging channel makes with reality so far appears marginal. An important motivation for this study is to see if this impression can be ameliorated through establishing that Tutty's waves are connected to the Jeffery–Hamel flows. This would imply that the theory of an infinitely diverging channel does have something more to say about practical flows.

It seems clear that any connection between Tutty's waves and Jeffery–Hamel flows is not through a local bifurcation. The linear spatial stability of Jeffery–Hamel flows to small steady two-dimensional perturbations of the streamfunction, with independent modes proportional to $r_*^{\lambda} = \mathrm{e}^{\lambda\rho}$, is governed by the Dean problem (see Banks *et al.* 1988), which determines λ as a complex eigenvalue. Marginal stability occurs where $\mathrm{Re}(\lambda) = 0$. Calculations suggest that $\lambda = 0$ wherever $\mathrm{Re}(\lambda) = 0$, that is to say the principle of exchange of (spatial) stabilities is valid. This *linear* result suggests that there is no local bifurcation of a Jeffery–Hamel flow to a spatially periodic flow, and that therefore continuation of Tutty's waves by decreasing (or increasing) the Reynolds number will not give a Jeffery–Hamel solution.

Tutty (1996) did not attempt to calculate the approximately periodic waves systematically. He investigated the flow near (α_2, Re_2) over a range of values, and reported representative results for a few values with small semi-angle α (1°, 2° and 5.73°) and Reynolds numbers of $O(100)$. Since Jeffery–Hamel flows asymptote to plane Poiseuille flow as $\alpha \to 0$, it is natural to ask how Tutty's waves may relate to the travelling wave solutions now known there (Zahn *et al.* 1974; Ehrenstein & Koch

1991). Of course, there are other questions such as: over what ranges of α and Re do these waves exist, how are they born and what happens to them, that is, what is the bifurcation structure of Tutty's waves as α and Re are varied?

To find answers to these questions, we first seek to establish the existence of Tutty's waves in the infinitely diverging channel idealization. The appropriate partial-differential boundary-value problem is set up in § 2 to find them economically. This problem is solved numerically and the numerical results interpreted in § 3 and § 4. The waves are found, leaving no doubt of their existence, although the evidence for their existence is only numerical. Their bifurcation structure is unfolded by use of path-continuation software. The overall conclusions are presented in § 5.

2. The mathematical problem

The dimensional vorticity equation for unsteady two-dimensional flow of an incompressible viscous fluid is well-known to be

$$\nu\nabla_*^2\zeta_* + \frac{1}{r_*}\frac{\partial(\psi_*, \zeta_*)}{\partial(r_*, \theta)} = \frac{\partial\zeta_*}{\partial t_*}, \tag{2}$$

where the streamfunction is ψ_* and the vorticity is

$$\zeta_* = -\nabla_*^2\psi_*. \tag{3}$$

Here the velocity components of the flow are $u_r = r_*^{-1}\partial\psi_*/\partial\theta$, $u_\theta = -\partial\psi_*/\partial r_*$, and ∇_*^2 is the Laplacian. The boundary conditions at the rigid walls of the Jeffery–Hamel problem are

$$\psi_* = \pm\tfrac{1}{2}Q, \quad \partial\psi_*/\partial\theta = 0 \quad \text{at} \quad \theta = \pm\alpha. \tag{4}$$

The dimensionless vorticity equation becomes

$$\frac{1}{Re}\nabla^2\zeta + \frac{1}{r}\frac{\partial(\psi, \zeta)}{\partial(r, \theta)} = \frac{\partial\zeta}{\partial t}, \tag{5}$$

where $r := r_*/r_0$, $t := \frac{1}{2}t_*Q/r_0^2$, $\psi := 2\psi_*/Q$, r_0 is an arbitrary length scale,

$$\zeta = -\nabla^2\psi, \tag{6}$$

and the dimensionless Laplacian operator is

$$\nabla^2 := \frac{1}{r}\frac{\partial}{\partial r}\left(\frac{\partial}{\partial r}\right) + \frac{1}{r^2}\frac{\partial^2}{\partial\theta^2}.$$

The boundary conditions are

$$\psi = \pm 1, \quad \partial\psi/\partial\theta = 0 \quad \text{at} \quad \theta = \pm\alpha. \tag{7}$$

Following Tutty's (1996) work, we assume that there are solutions of period $2\pi/\omega$ in $\rho := \log r_*$, and define new coordinates

$$X := \omega\log(r_*/r_0), \quad Y := \theta/\alpha, \tag{8}$$

where the wavenumber ω has to be determined and r_0 may be regarded as the distance from the origin of the periodic wave cell, $r_0 < r_* < r_0 e^{2\pi/\omega}$ or $0 < X < 2\pi$. Therefore $\nabla^2 = \alpha^{-2}e^{-2X/\omega}\mathrm{D}^2$, where

$$\mathrm{D}^2 := \frac{\partial^2}{\partial Y^2} + \alpha^2\omega^2\frac{\partial^2}{\partial X^2},$$

and so

$$\zeta = -\frac{1}{\alpha^2} e^{-2X/\omega} D^2 \psi. \tag{9}$$

Substitution of this expression into equation (5) yields

$$D^2\zeta + \alpha\omega Re \frac{\partial(\psi, \zeta)}{\partial(X, Y)} = \alpha^2 Re\, e^{2X/\omega} \frac{\partial \zeta}{\partial t}. \tag{10}$$

Boundary conditions (7) become

$$\psi = \pm 1, \quad \partial\psi/\partial Y = 0 \quad \text{at} \quad Y = \pm 1. \tag{11}$$

Equations (9) and (10) over the domain $\Omega = \{(X, Y) : 0 < X < 2\pi, -1 < Y < 1\}$, with boundary conditions (11) and the periodicity of 2π in X, define the problem to be solved. The aim is to find solutions (ω as well as ψ and ζ) for given values of Re, α. Of course, the Jeffery–Hamel flows themselves (for which ψ is independent of X and t, and ω is arbitrary) are special solutions.

It is convenient to define and use a transformed dependent variable,

$$Z := \alpha^2 e^{2X/\omega} \zeta, \tag{12}$$

so that equations (9) and (10) become

$$D^2\psi = -Z \tag{13}$$

and

$$D^2 Z - 4\alpha^2\omega \frac{\partial Z}{\partial X} + 4\alpha^2 Z + \alpha Re \left[\omega \frac{\partial(\psi, Z)}{\partial(X, Y)} + 2\frac{\partial \psi}{\partial Y} Z\right] = \alpha^2 Re\, e^{2X/\omega} \frac{\partial Z}{\partial t}. \tag{14}$$

To focus on the calculation of Tutty's steady periodic waves, we further assume that ψ is independent of t so that

$$D^2 Z - 4\alpha^2\omega \frac{\partial Z}{\partial X} + 4\alpha^2 Z + \alpha Re \left[\omega \frac{\partial(\psi, Z)}{\partial(X, Y)} + 2\frac{\partial \psi}{\partial Y} Z\right] = 0, \tag{15}$$

and ψ also satisfies the symmetry condition

$$\psi(X + \pi, -Y) = -\psi(X, Y) \tag{16}$$

for all $(X, Y) \in \Omega$. This symmetry condition exploits Tutty's results by effectively halving the computational domain, but at the cost of excluding the discovery of solutions without this symmetry.

We have used a spectral method to solve the nonlinear partial-differential boundary-value problem (13), (15), (11), (19) and (16) numerically. The essence of the method is to take a Fourier expansion of ψ and Z in X and a Chebyshev expansion in Y to reduce the problem to a nonlinear algebraic problem. The algebraic problem is then truncated and solved by Newton–Raphson approximation and a path-following algorithm; we used the software package PITCON (Rheinboldt & Burkardt 1983*a*, *b*), to do this. The spectral method may be sketched as follows. Expand

$$\psi(X, Y) = \sum_{n=0}^{N-1} a_n T_{2n+1}(Y) + \sum_{m=-M, m\neq 0}^{M} \sum_{n=0}^{N-1} b_{mn} e^{imX} \phi_n^{(m)}(Y), \tag{17}$$

$$Z(X, Y) = \sum_{n=0}^{N-1} c_n T_{2n+1}(Y) + \sum_{m=-M, m\neq 0}^{M} \sum_{n=0}^{N-1} d_{mn} e^{imX} \phi_n^{(m)}(Y), \tag{18}$$

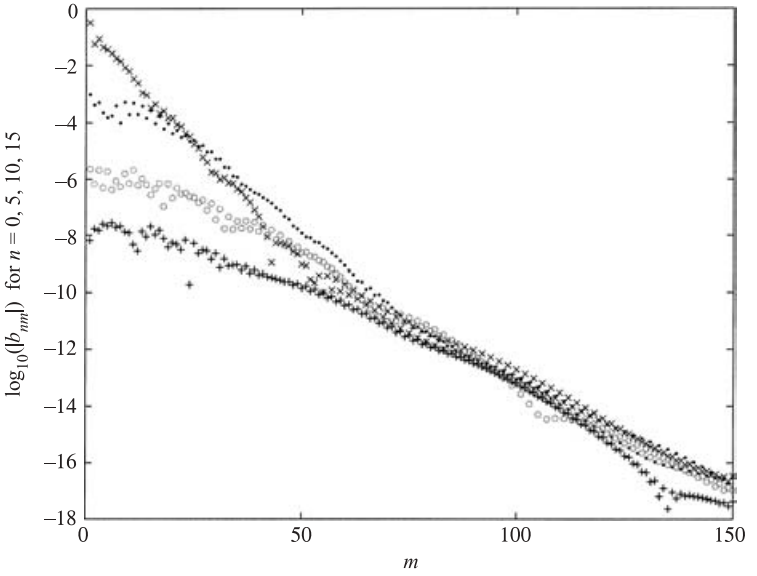

FIGURE 3. Spectral convergence: $\log_{10}$ of the modulus of the coefficients b_{m0} ($\times$), b_{m5} ($\cdot$), b_{m10} ($\circ$) and b_{m15} ($+$) for the streamfunction at $(\alpha, Re) = (0.1, 45)$ are plotted verses m, the spectral degree (see the representation in equation (17)) calculated using $(N, M) = (20, 150)$.

where the positive integers M, N are truncation parameters, to be taken as large as is practical, $T_n(Y) = \cos[n \cos^{-1}(Y)]$ is the Chebyshev polynomial of degree n, and

$$\phi_n^{(m)}(Y) := \begin{cases} T_{2n}(Y) & m \text{ odd} \\ T_{2n+1}(Y) & m \text{ even} \end{cases}$$

in order to satisfy the symmetry (16). For the solutions to be real,

$$b_{-mn} = b_{mn}^*, \quad d_{-mn} = d_{mn}^*,$$

where an asterisk denotes complex conjugation. The problem is invariant under translations in X, so, to make the solution unique (at least in a given neighbourhood of phase space), we may impose a phase condition

$$\mathrm{Re}(\mathrm{e}^{\mathrm{i}\beta} b_{10}) = 0 \tag{19}$$

where β is a constant set by Tutty's initial data, to fix the position of the wave relative to $X = 0$. On equating coefficients of $\mathrm{e}^{\mathrm{i}mX}$ and $T_n(Y)$ in equations (11), (13), (15) and (19), this reduces the problem to a nonlinear algebraic problem for solutions specified by the real coefficients $\{a_n\}, \{c_n\}$ and the complex coefficients $\{b_{mn}\}, \{d_{mn}\}$.

3. Results

Our investigation was initiated by taking unpublished wave data found by Tutty (1996) at $(\alpha, Re) = (0.1, 45)$, converting it into the spectral representation (defined by expressions (17) and (18)) and using this as a starting guess for a Newton–Raphson scheme to solve the nonlinear problem for the spectral coefficients a_n, b_{mn}, c_n, d_{mn}. The fact that we obtained robust spectral (exponential) convergence over a range of truncations ($8 < N < 20$, $30 < M < 200$ – see figure 3) confirmed that the wave existed in the infinitely diverging channel idealization. Once convergence had been

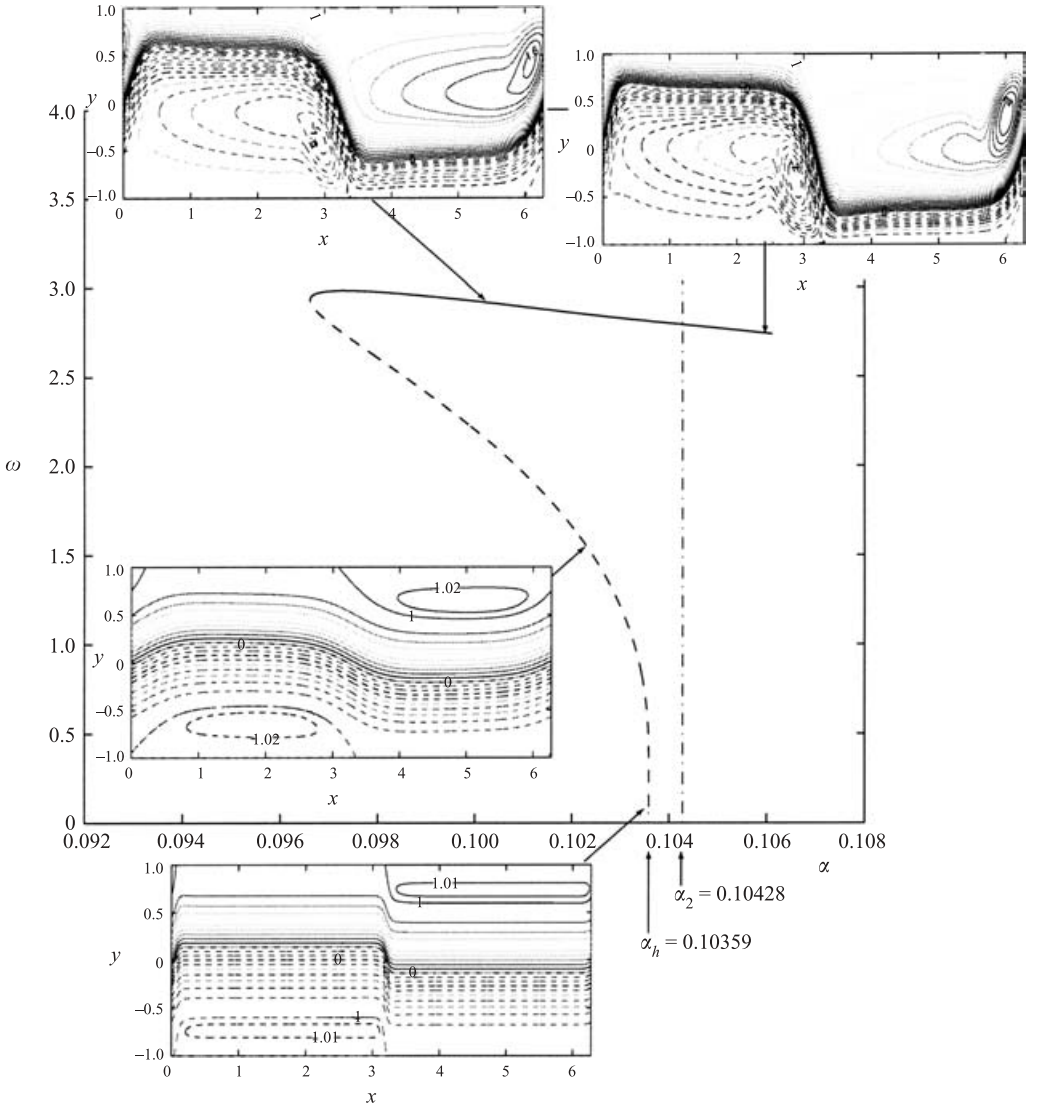

FIGURE 4. Bifurcation diagram of ω versus α for $Re = 45$. The insets are contour plots of the streamfunction at the indicated points on the solution branch. Starting at the top and working downwards, $(\alpha, \omega) = (0.1, 2.925)$ (Tutty's initial data), $(\alpha, \omega) = (0.106114, 2.73957)$, $(\alpha, \omega) = (0.10244, 1.489)$ and $(\alpha, \omega) = (0.103587, 0.11813)$. All contour intervals are 0.1: the lower two plots have extra contours with values 1.02 and 1.01 added.

established, one of the variables Re, α, ω was fixed, a second was varied and the third allowed to be defined as part of the solution-finding procedure. In this way, the two-dimensional surface of wave solutions in (α, Re, ω)-space was traced out. All results were extensively checked by rerunning with different truncations. This proved essential as the necessary truncation levels varied so much (see below) along a typical solution branch.

Figure 4 shows the result of fixing the Reynolds number at $Re = 45$ and continuing the wave solution in α from Tutty's initial data at $\alpha = 0.1$. The waves are clearly found to exist at α values beyond $\alpha_2(Re = 45) = 0.10428$ but become hard to follow here as

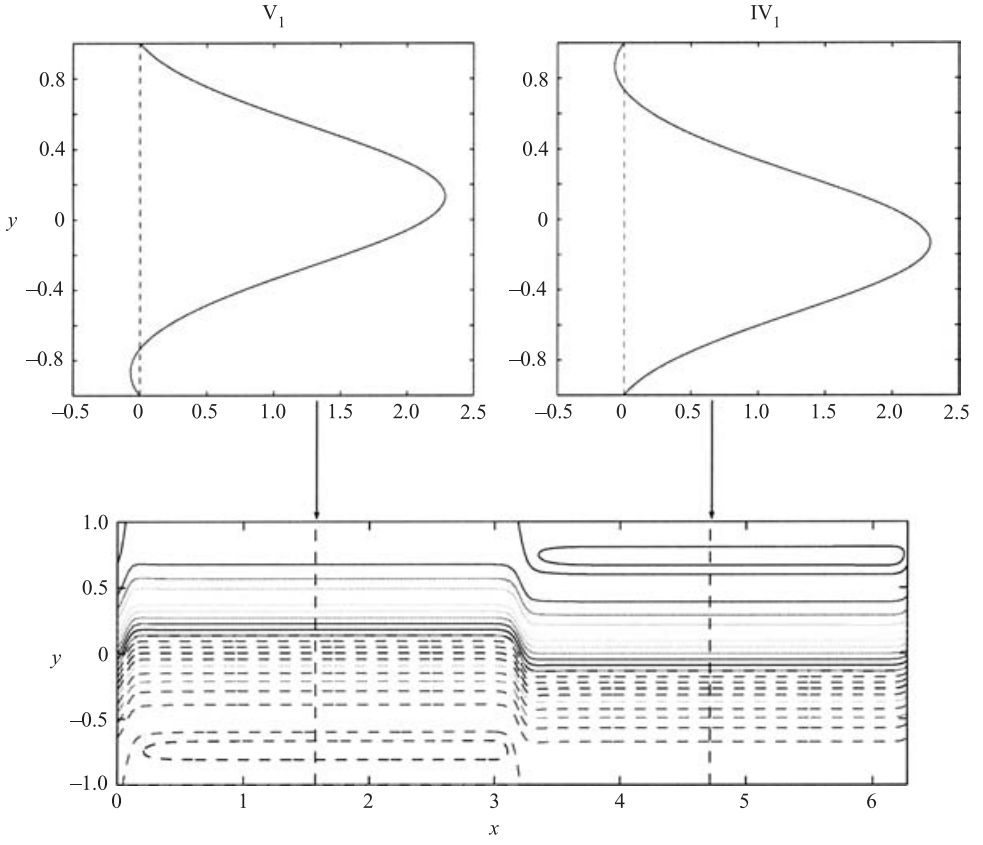

FIGURE 5. Two cross-sectional slices across the lowest $((\alpha, \omega) = (0.103587, 0.11813))$ contour plot in figure 4. These indicate that the regions of one-dimensional flow either side of the rapid transition layer correspond very closely to the states IV_1 and V_1. On the upper plots, the abscissa is $d\psi/dy$ which is proportional to u_r.

interior cross-stream (Y) gradients in the streamfunction become large (the required truncation at $\alpha \approx 0.106$ was $(N, M) = (25, 50)$ compared to just $(N, M) = (10, 50)$ at $\alpha = 0.1$). When α is reduced below 0.1, the waves undergo a saddle-node bifurcation at $(\alpha, \omega) \approx (0.0966, 3)$ and then $\omega \to 0$ as $\alpha \to \alpha_h \approx 0.1036$. In order to estimate α_h, the streamwise (X) truncation had to be increased considerably from $M = 50$, with $M = 250$ the largest value used. However large M was taken, the numerically continued branch of solutions would monotonically approach α_h before then oscillating and turning away to lower α values. These latter 'solutions' were always spurious, being strongly dependent on the particular truncation employed. Crucially the smallest value of ω at which 'true' converged solutions could be secured decreased inversely with the truncation level used. This indicated that the smallest streamwise lengthscale present in the wave solution was $O(\omega)$ in the computational domain $0 \leqslant X \leqslant 2\pi$ or equivalently $O(1)$ in the physical domain of $0 \leqslant \log(r_*/r_0) \leqslant 2\pi/\omega$. The contour plot insets on figure 4 show how the streamfunction increasingly divides into two different regions with no cross-stream flow matched through a thin transitory layer as $\alpha \to \alpha_h$. Measurements confirm that this transition layer is $O(\omega)$ thick and figure 5 shows that the two flows linked through this layer are very similar to the asymmetric Jeffery–Hamel states IV_1 and V_1.

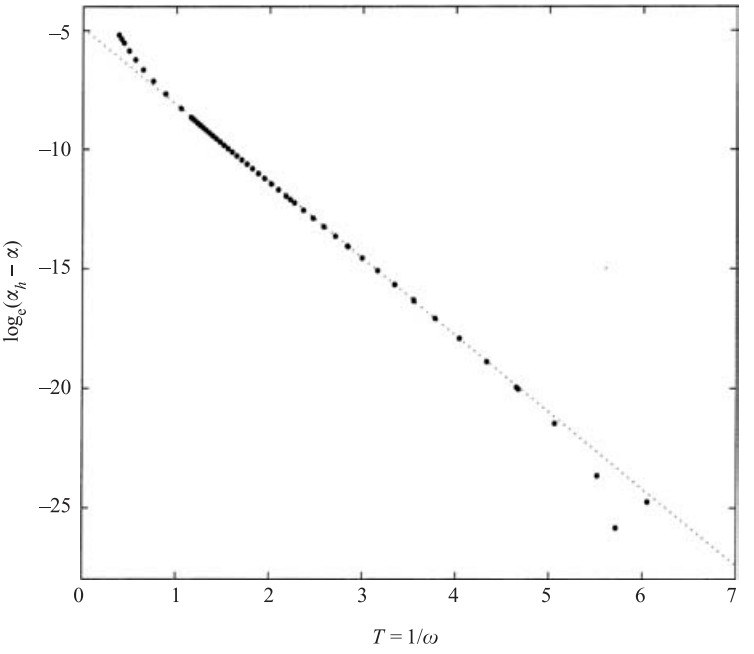

FIGURE 6. This plot demonstrates that the limit-cycle period scales logarithmically with the distance from the heteroclinic bifurcation point, that is, $\alpha_h - \alpha \sim Ae^{-\lambda/\omega}$. The best fit line has $\lambda = 3.22$, $Re = 45$ and the data come from a $(N, M) = (10, 200)$ run. Loss of numerical accuracy is responsible for the drift off the best fit line at small values of ω.

Based on the evidence so far it seems reasonable to hypothesize that the wave branch does connect with the $\omega = 0$ axis at a distinquished point $\alpha = \alpha_h$ and that here the flow solution represents a heteroclinic connection across the subcritical pitchfork arms of the Jeffery–Hamel bifurcation centred at $\alpha = \alpha_2$. In this scenario, Tutty's wave (or the continuation thereof) corresponds to the limit cycle born out of a heteroclinic bifurcation (interpreting the streamwise coordinate X as the time variable). This is certainly supported by finding the characteristically logarithmic scaling of the limit cycle (spatial) period $(2\pi/\omega)$ with distance from the heteroclinic bifurcation $(\alpha_h - \alpha)$ – see figure 6. However, there is the alternative possibility that Tutty's waves result from a codimension-2 point in (α, Re)-space and that $(\alpha, Re) = (0.1036, 45)$ is close to that. Revisiting the Dean spatial stability problem fails to ever find more than one eigenvalue becoming marginal along the curve $\alpha = \alpha_2(Re)$. To further confirm that the bifurcation is not localized in (α, Re)-space, the branch of wave solutions existing at $Re = 45$ can easily be extended over the Reynolds number range $10 \leqslant Re \leqslant 5000$. Figure 7 shows cross-sections of the wave solution surface at four different Reynolds numbers (figure 8 shows contour plots of the streamfunctions at two points on the $Re = 10$ and $Re = 100$ cross-sections). Capturing the saddle-node point on these curves becomes increasingly difficult as Re increases, until beyond about $Re = 1000$ the required truncation becomes too expensive. However, it is clear that α_s, the value of α which corresponds to the saddle nose, asymptotically approaches α_2 which itself approaches $4.712/Re$ as $Re \to \infty$. This means that the wave branch never pierces the $\alpha = 0$ axis which at fixed Re corresponds to the plane Poiseuille limit. This is perhaps not surprising given that only travelling wave solutions are known to exist there rather than the steady waves discussed here.

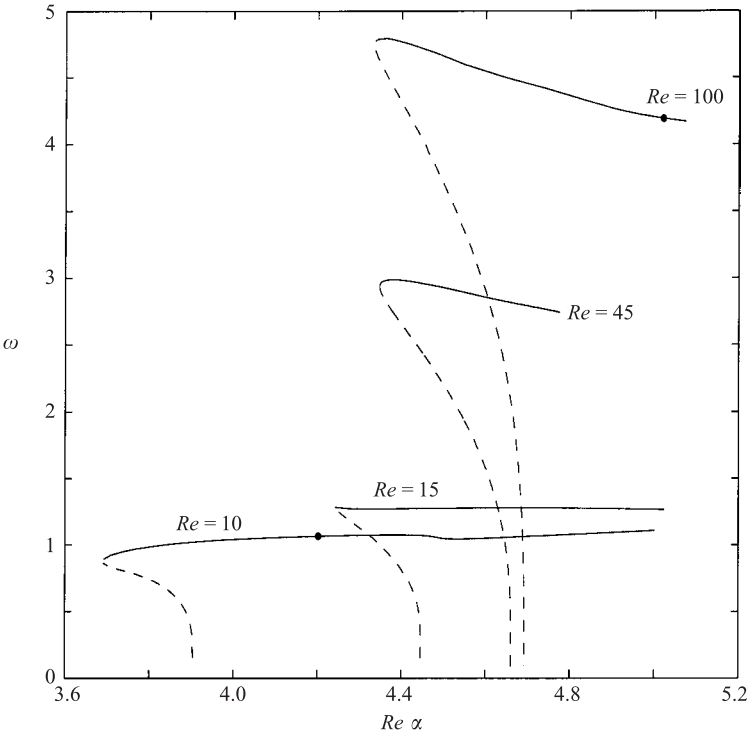

FIGURE 7. Four cross-sections of the wave solution surface in (α, Re, ω)-space at $Re = 10, 15, 45$ and 100. The solutions below the saddle-nose point are inferred spatially unstable (dashed line) as opposed to those above, which are presumed stable (solid line). The two dots indicate the parameter values at which the streamfunction contour plots of figure 8 have been produced.

Interestingly, over the range $5 \leqslant Re \leqslant 100$ where there is sufficient numerical accuracy available, the normalized distance between the pitchfork nose and the inferred heteroclinic bifurcation point, $(\alpha_2 - \alpha_h)/\alpha_2$, is found to scale like Re^{-2} – see figure 9. This suggests that the asymptotic limit $Re \to \infty$ may offer more insight into the situation.

3.1. *Asymptotic limit* $Re \to \infty$

To explore the limit $Re \to \infty$, we work with the expansion parameter

$$0 < \delta^2 := \frac{\alpha_2 - \alpha_h}{\alpha_2} \ll 1 \tag{20}$$

which measures the (small) distance of the heteroclinic connection to the pitchfork nose, and the governing equations

$$\mathrm{D}^2 Z - 4\alpha_2^2 \frac{\partial Z}{\partial x} + 4\alpha_2^2 Z + \alpha_2 Re \left[\frac{\partial(\psi, Z)}{\partial(x, y)} + 2\frac{\partial \psi}{\partial y} Z \right] = 0 \tag{21}$$

and

$$Z = -\mathrm{D}^2 \psi = -\left(\frac{\partial^2}{\partial y^2} + \alpha_2^2 \frac{\partial^2}{\partial x^2} \right) \psi \tag{22}$$

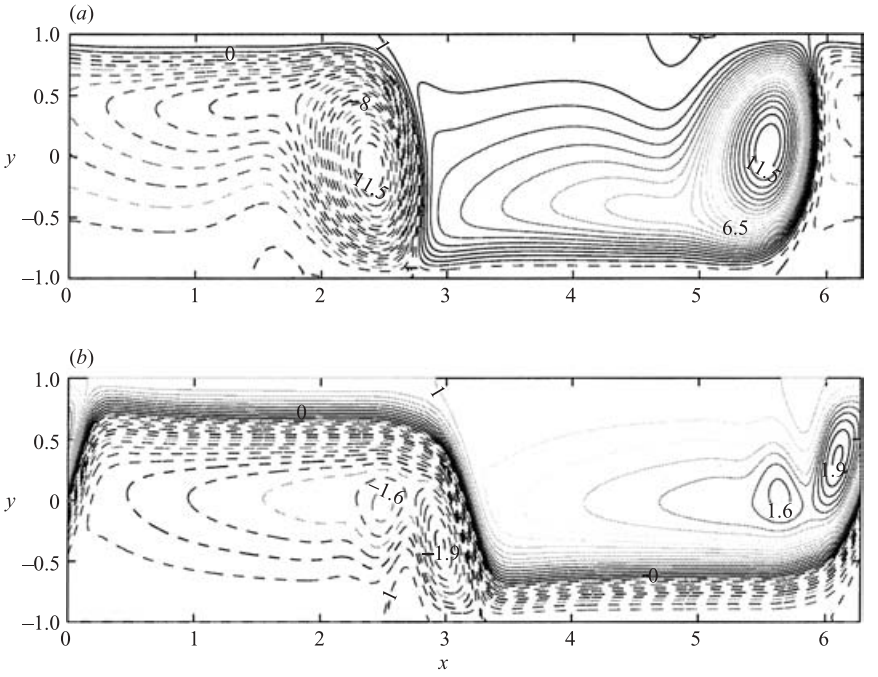

FIGURE 8. Contour plots of the streamfunctions at the two dots in figure 7: (*a*) corresponds to $(\alpha, Re, \omega) = (1.064772, 9.7245, 0.4202)$ with contour intervals of 0.5 to a maximum of 11.5 (dashed lines indicating negative values), and (*b*) corresponds to $(\alpha, Re, \omega) = (0.05003, 100.204, 4.1691)$ with contour intervals of 0.1 to a maximum of 1.9.

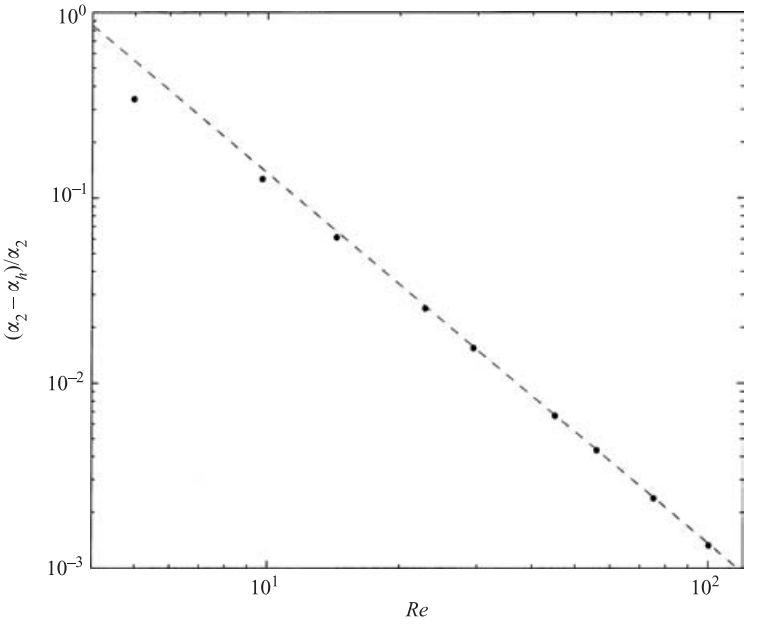

FIGURE 9. A plot of $(\alpha_2 - \alpha_h)/\alpha_2$ against Re indicating $O(Re^{-2})$ asymptotic behaviour. The best fit line is $13.6Re^{-2}$.

where $x = X/\omega$ to remove the implicit periodicity implied by ω and $y := \theta/\alpha_2$ so that now the boundary conditions are

$$\psi(x, \pm(1-\delta^2)) = \pm 1, \quad \psi_y(x, \pm(1-\delta^2)) = 0. \tag{23}$$

As in the weakly nonlinear analysis of Banks *et al.* (1988), an asymptotic expansion of the form

$$\psi = G_0(y;\alpha_2) + \delta G_1(x, y) + \delta^2 G_2(x, y) + \delta^3 G_3(x, y) + \dots \tag{24}$$

is opened up with $G_0(y;\alpha_2)$ corresponding to the (known) flow solution II_1 precisely at the pitchfork nose so that $G_{0,yy}(y;\alpha_2) = 0$. Taylor-expanding the boundary conditions then requires

$$G_1 = G_{1,y} = G_2 = G_{2,y} = 0, \quad G_3 = G_{1,y}, \quad G_{3,y} = G_{1,yy} \quad \text{at } y = \pm 1. \tag{25}$$

It is clear from the ensuing hierarchy of ordered equations that δ must scale with α_2 or equivalently Re^{-1} as

$$\alpha_2 \sim \frac{\mu_0}{Re} + \frac{\mu_1}{Re^2} + \dots \quad \text{as } Re \to \infty \tag{26}$$

(where $\mu_0 = 4.712$) if the effects of streamwise dependence are to contribute at the right order. We now explain this claim.

The leading $O(1)$ problem defined by (21) and (22) and with the term $4\alpha_2^2 Z$ promoted in the ordering is

$$G_{0,yyyy} + 4\alpha_2^2 G_{0,yy} + 2\alpha_2 Re\, G_{0,y} G_{0,yy} = 0 \tag{27}$$

which with the boundary conditions $G_0(\pm 1) = \pm 1$ and $G_{0,y}(\pm 1) = 0$ specifies the Jeffery–Hamel flow II_1 at the pitchfork nose. At $O(\delta)$

$$\mathscr{L} G_1 := G_{1,yyyy} + 4\alpha_2^2 G_{1,yy} + \mu_0[2(G_{0,y}G_{1,y})_{,y} + G_{0,yyy}G_{1,x} - G_{0,y}G_{1,xyy}] = 0 \tag{28}$$

with $G_1(x, \pm 1) = G_{1,y}(x, \pm 1) = 0$. If G_1 is temporarily imagined independent of x, this problem defines the structure (but not amplitude) of the asymmetric state which defines the pitchfork arm (as $\alpha \to \alpha_2$) and is known to be proportional to $G_{0,y}(y;\alpha_2)$. Interestingly, because of the special structure of the operator which premultiplies the x-derivative, the full solution is

$$G_1(x, y) = A(x) G_{0,y}(y;\alpha_2) \tag{29}$$

where $A(x)$ remains undefined up to the obvious boundary condition, $A(-\infty) = -A(\infty)$ for a heteroclinic connection across the pitchfork arms. This is confirmed by the numerical solutions which indicate that $A(x)$ has a tanh-like behaviour. One would imagine that an amplitude equation for $A(x)$ would emerge through the first non-trivial application of the Fredholm Alternative to a higher-order problem. This, after all, is how the amplitude of the pitchfork arms, $A(\pm\infty)$, is found as a function of the distance away from the bifurcation point $(\alpha_2 - \alpha)/\alpha_2$ (Banks *et al.* 1988). However the addition of the x-derivative crucially converts $\mathscr{L}$ from being an elliptic operator in y into a parabolic operator in x and y. This means that no solvability condition exists for the higher-order problems which take the form $\mathscr{L} G_n = f(G_0, G_1, \dots, G_{n-1})$. A further indication of this is the fact that the dimension of the null space of the adjoint of $\mathscr{L}$ is smaller than for $\mathscr{L}$ itself. This fatal flaw in the perturbative analysis attempted here is nothing more than a manifestation of the fact that the heteroclinic bifurcation is a global rather than local phenomenon. However, at least we can understand the

scalings by this procedure so we press onto the $O(\delta^2)$ problem

$$\mathscr{L}G_2 = \mu_0[\, G_{1,y}G_{1,xyy} - G_{1,x}G_{1,yyy} - 2G_{1,y}G_{1,yy}\,] \tag{30}$$

with $G_2(x, \pm 1) = G_{2,y}(x, \pm 1) = 0$. Only the last term on the right is present in the weakly nonlinear Jeffery–Hamel analysis but the two new x-derivative terms also share the same y-symmetry so G_2 is antisymmetric in y whereas G_1 is symmetric in y. This familiar situation means that the pitchfork analysis must proceed to the next order to obtain a non-trivial solvability condition. The scaling $\alpha_2^2 = \lambda\delta^2$ (i.e. $\delta = O(Re^{-1})$) ensures that the lowest-order terms due to x-variation with the same symmetry in y as G_1 emerge at precisely this order. Ignoring terms without this symmetry, the problem at $O(\delta^3)$ is

$$\begin{aligned}\mathscr{L}G_3 = {} & -2\lambda G_{1,xxyy} + 4\lambda G_{1,xyy} + \mu_0[\, G_{1,y}G_{2,xyy} + G_{1,xyy}G_{2,y} - G_{1,x}G_{2,yyy} \\ & - G_{1,yyy}G_{2,x} + \lambda G_{0,y}G_{1,xxx} - 2\lambda G_{0,y}G_{1,xx} - 2G_{1,y}G_{2,yy} - 2G_{1,yy}G_{2,y}] \end{aligned} \tag{31}$$

with $G_3(x, \pm 1) = 0$ and $G_{3,y}(x, \pm 1) = A(x)G_{0,yyy}(\pm 1; \alpha_2)$. Presumably only one (positive) value of the free coefficient λ will ensure that the solution G_3 smoothly asymptotes to the right y-dependent function at either pitchfork arm. Resolving this means tackling the full partial differential equation which reflects the global nature of the heteroclinic connection. We can, however, motivate a much simplified model of the situation to demonstrate that the dynamical picture advocated here is at least plausible. The first simplification is motivated by the fact that $G_2(x, y) = \frac{1}{2}A^2(x)G_{0,yy}$ is a particular solution to (30) which only falls short of being the complete solution through failing to satisfy the derivative boundary conditions $G_{2,y}(x, \pm 1) = 0$. Choosing to assume that $G_2(x, y) = A^2(x)\hat{G}_2(y)$ nevertheless allows us to apply a solvability-like procedure to (31). This consists of forming the integral $\langle G_{0,y}, (31)\rangle := \int_{-1}^{1} G_{0,y}\,(31)\,\mathrm{d}y$ which gives

$$\begin{aligned}\langle G_{0,y}, \mathscr{L}G_3\rangle = {} & \mu_0\lambda\big\langle G_{0,y}, G_{0,y}^2\big\rangle A_{xxx} - 2\lambda\big\langle G_{0,y}, G_{0,yyy} + \mu_0 G_{0,y}^2\big\rangle A_{xx} \\ & + 4\lambda\langle G_{0,y}, G_{0,yyy}\rangle A_x + \mu_0\langle G_{0,y}, 2G_{0,yy}\hat{G}_{2,yy} + G_{0,yyy}\hat{G}_{2,y} - G_{0,y}\hat{G}_{2,yyy} \\ & - 2G_{0,yyyy}\hat{G}_2\rangle A^2 A_x - 2\mu_0\langle G_{0,y}, 2G_{0,yy}\hat{G}_{2,yy} + 2G_{0,yyy}\hat{G}_{2,y}\rangle A^3. \end{aligned} \tag{32}$$

In the true solvability situation, the left-hand-side integral can be straightforwardly evaluated by acting with the adjoint of $\mathscr{L}$ on $G_{0,y}$. However here we are forced to ignore the x-derivative part of the operator in $\mathscr{L}$ so that $\langle G_{0,y}, \mathscr{L}G_3\rangle \propto A$. After further ignoring the A_{xxx} term, this can be rewritten in the general form

$$A_{xx} = (\alpha - \alpha_2)A + A^3 - \epsilon A_x(1 - A^2) \tag{33}$$

where for convenience we have set some of the coefficients to 1 and labelled another by ϵ since this is only a heuristic model (actually this equation captures a generic type of behaviour near a Takens–Bogdanov bifurcation point with symmetry; e.g. see Guckenheimer & Holmes 1983). For $\epsilon \neq 0$, the system can be viewed as the perturbed Hamiltonian system

$$\dot{q} = p, \tag{34}$$

$$\dot{p} = (\alpha - \alpha_2)q + q^3 - \epsilon p(1 - q^2), \tag{35}$$

where $q = A$ and an overdot represents differentiation with respect to x. When $\epsilon = 0$, the system is Hamiltonian ($H = \frac{1}{2}p^2 - \frac{1}{2}(\alpha - \alpha_2)q^2 - \frac{1}{4}q^4$) and there are heteroclinic connections between the two saddles at $q = \pm(\beta := \sqrt{\alpha_2 - \alpha})$ for $\alpha - \alpha_2 < 0$. The

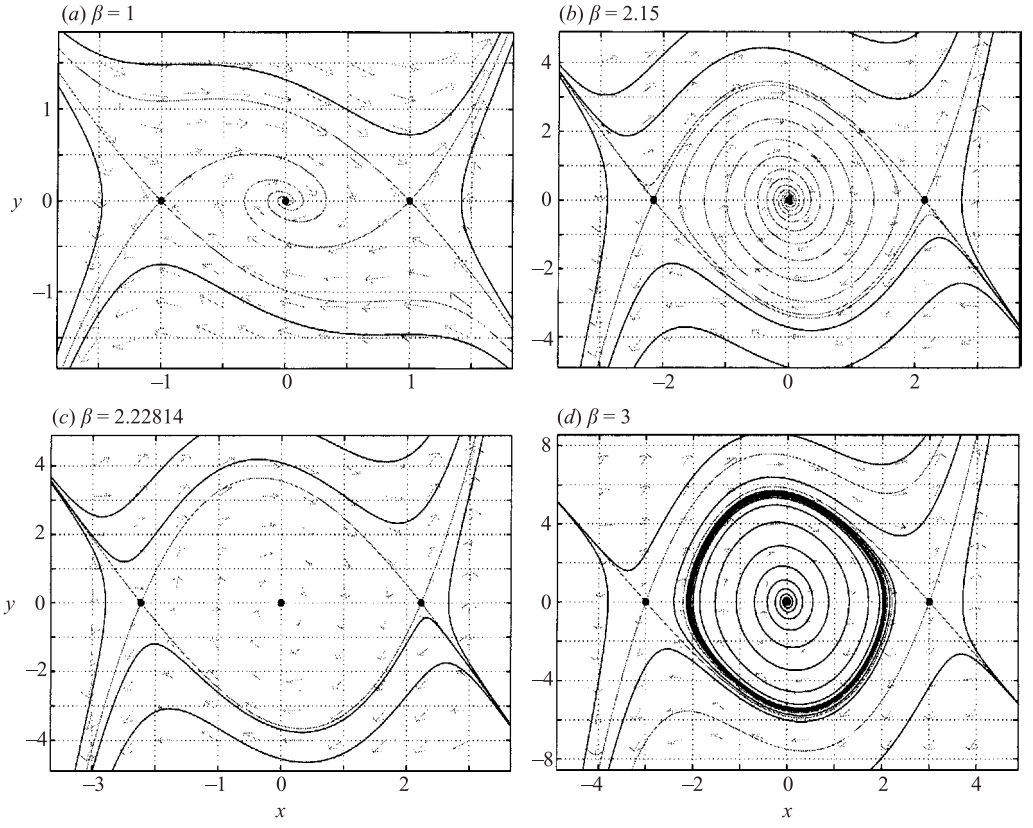

FIGURE 10. Phase planes for the model system $\dot{q} = p$, $\dot{p} = -\beta^2 q + q^3 - 0.5p(1-q^2)$: $\epsilon = 0.5$ for greater clarity and $q = x$ and $p = y$). Throughout the origin is a stable spiral. (*a*) $\alpha_h < \alpha < \alpha_2$; (*b*) $\alpha_h \lesssim \alpha < \alpha_2$; (*c*) the heteroclinic connection at $\alpha = \alpha_h$; (*d*) an unstable limit cycle is born for $\alpha < \alpha_h$.

'upper' ($p \geqslant 0$) connection is

$$q_h(x;\beta) := \beta \frac{e^{\sqrt{2}\beta x} - 1}{e^{\sqrt{2}\beta x} + 1}, \qquad p_h(x,\beta) := \frac{2\sqrt{2}\beta^2 e^{\sqrt{2}\beta x}}{(e^{\sqrt{2}\beta x} + 1)^2}. \tag{36}$$

For $\epsilon > 0$, Melnikov theory predicts that a heteroclinic connection will be re-established in the asymptotic limit of $\epsilon \to 0$ when the function

$$M(\beta) := \int_{-\infty}^{\infty} p_h^2(x;\beta)\big(1 - q_h^2(x;\beta)\big)\,\mathrm{d}x \tag{37}$$

vanishes. This occurs very close to $\beta = \sqrt{5}$ or $\alpha_2 - \alpha \approx 5$. Figure 10 shows the change in topology of the phase plane as α varies ($\epsilon = 0.5$ for clarity and as a result $\alpha_2 - \alpha_h = 4.964$ rather than 5). We believe this models the situation in the full diverging channel system.

4. Extended channel calculations

A number of numerical calculations were performed in an extended channel without assuming periodicity to confirm the picture of the flow given above. A particular

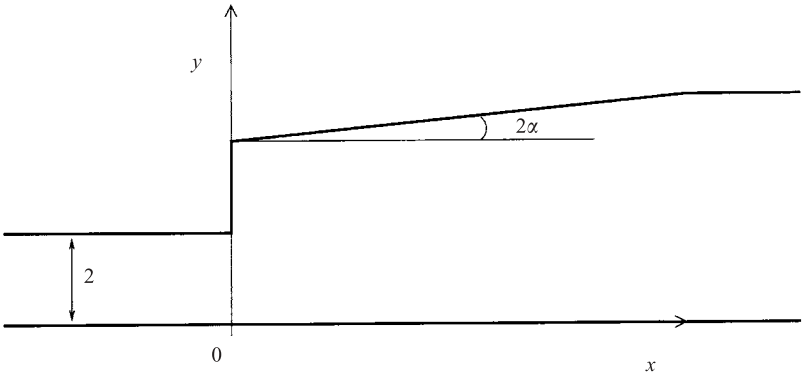

FIGURE 11. Channel geometry (not to scale).

motivation was to test the spatial stability of the various branches of the bifurcation diagrams shown in figures 4 and 7.

The code used was a steady version of that detailed in Tutty & Pedley (1993), which was also used by Tutty (1996). Initially, the geometry considered was the same as in Tutty (1996), as shown in figure 11. The channel has an upstream region of non-dimensional width 2, with parallel walls so that Poiseuille flow can be used at the inlet, then a step on the upper wall of the channel, followed by a long region with the upper wall inclined at an angle of 2α, with a flat lower wall. Far downstream, the channel walls revert to parallel, for reasons of numerical stability. This downstream region does not have any significant effect on the development of the flow/wave over most of the channel. The calculations were performed in a uniform channel of width 2, which was mapped onto the non-uniform channel shown in figure 11 using a combination of an exponential transformation, which maps the uniform channel to a half-plane, followed by a Schwarz–Christoffel transform which maps the half-plane to the physical channel. The result is a conformal transformation between $\hat{Z} = \hat{X} + \mathrm{i}\hat{Y}$ and $z = x + \mathrm{i}y$ where $(\hat{X}, \hat{Y})$ is the computational space and (x, y) physical space. Details can be found in Tutty (1996). Note however that the mapping has been adjusted so that here the computational domain has $-1 \leqslant \hat{Y} \leqslant 1$, whereas in Tutty (1996) a channel of unit width was used.

In the main part of the channel where the walls are non-parallel, away from the points where the shape changes, the computational coordinate system reduces to

$$\hat{X} = X/(\alpha\omega), \quad \hat{Y} = Y, \tag{38}$$

where (X, Y) are given by (8) above. This is the appropriate coordinate system to view the wave in an extended channel as the periodic state will produce a wave of constant length and strength. In particular, the scaled vorticity

$$\hat{\zeta} = J\zeta = -\frac{\partial^2\psi}{\partial\hat{X}^2} - \frac{\partial^2\psi}{\partial\hat{Y}^2} \tag{39}$$

where $J = |\mathrm{d}z/\mathrm{d}Z|^2$, should show a periodic pattern in $\hat{X}$.

With a step that doubles the width of the channel when the shape changes, the behaviour of the solution was investigated near the nose shown in figure 4 ($\alpha \approx 0.0966$), with excellent agreement. For all $\alpha > 0.0966$, (0.097, 0.975, 0.1) a wave was generated downstream of the step, tending to a periodic state in the computational coordinates, which are essentially the same as (X, Y) in this paper (see Tutty 1996).

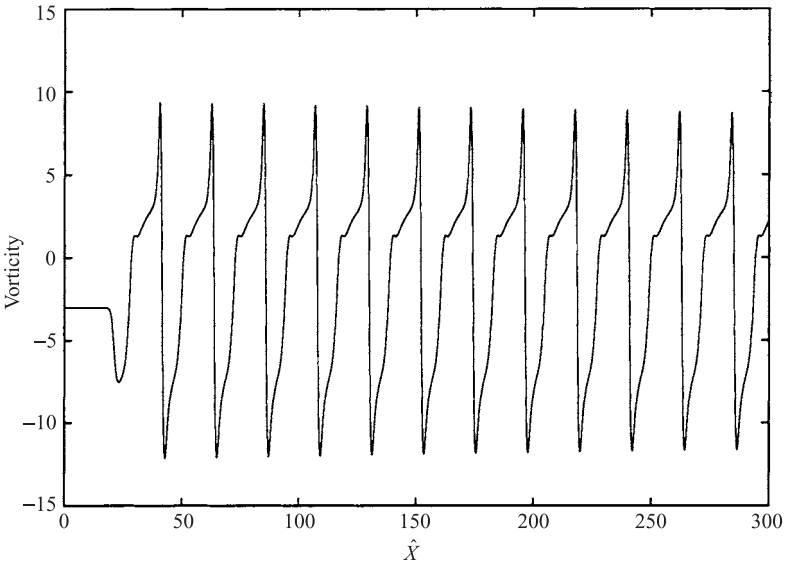

FIGURE 12. Scaled vorticity $\hat{\zeta}$ on the the lower wall for $Re = 45$, $\alpha = 0.0.0966$ for a channel with at step at $\hat{X} \approx 20$.

However, for $\alpha < 0.0966$ (0.0965, 0.964, 0.963, 0.962, 0.961 0.0960, 0.095), although a wave was generated by the step, it decayed with the flow, tending to the symmetric II_1 Jeffery–Hamel flow far downstream. With $\alpha = 0.0966$ there is an almost constant strength wave, as can be seen from figure 12, which shows the scaled vorticity $\hat{\zeta}$ on the lower wall against $\hat{X}$.

With the step geometry, attempts were made to generate solutions on the lower branch by stretching the upper-branch solution for a particular α, so that its wavelength approximately matched that on the lower branch as shown in figure 4, and using this as the initial condition for a new calculation. However, in all cases the converged solution was that found on the upper branch, supporting the idea that the lower branch is spatially unstable.

A further set of calculations was performed for a channel with a parallel region downsteam but not upstream. Again, the physical channel was mapped to a uniform computational channel, by dropping the appropriate part of the mapping outlined above for the channel shown in figure 11. At the inlet a Jeffery–Hamel flow was imposed. For $Re = 45$ and $\alpha = 0.10244$, one of the points shown on figure 4, if the Jeffery–Hamel flow at the inlet was the symmetric II_1 solution then there was no wave, and the II_1 solution was maintained downstream. However, if the inlet flow was the IV_1 Jeffery–Hamel flow, then a wave corresponding to that on the upper branch of figure 4 was generated. Further, if the converged solution with the wave was used as the starting condition for a calculation with the II_1 solution at the inlet, the final solution was that with II_1 downstream, i.e. the wave did not persist. In contrast, and as might be expected, using the converged II_1-type solution as the starting point of a calculation with IV_1 at the inlet, produced a wave. This pattern of behaviour was repeated for $Re = 500$ with $\alpha = 0.0091$, which is close to but below $\alpha_2 \approx 0.009424$. Again, the II_1 Jeffery–Hamel solution at the inlet did not produce a wave while the IV_1 solution did. Also, swapping the inlet conditions with the converged solutions swapped the final form of the solution.

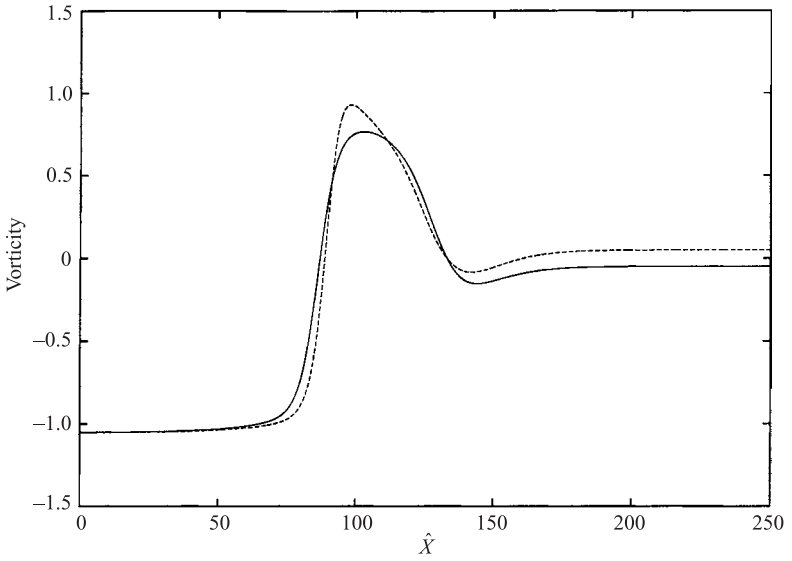

FIGURE 13. Scaled vorticity $\hat{\zeta}$ on the walls for $Re = 45$, $\alpha = 0.103587$, with the IV_1 flow at the inlet. The solid line is for the lower wall and the dashed line for the upper wall.

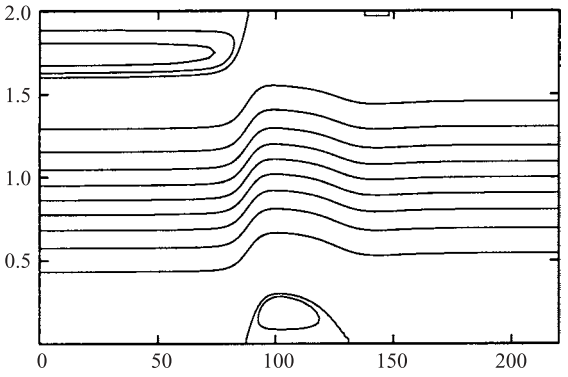

FIGURE 14. Streamlines for $Re = 45$, $\alpha = 0.103587$, with the IV_1 flow at the inlet. From the bottom the lines are for $\psi = -1.002$, -1 to 1 in steps of 0.2, 1.005 and 1.01.

The ability of the IV_1 inlet condition to produce the nonlinear wave on the upper branch, however, depended on being sufficiently far from the pitchfork nose. Being too close implies that the dynamics merely sit in the one-dimensional centre manifold of the pitchfork bifurcation where the flow would evolve from IV_1, which is spatially unstable (Banks *et al.* 1988) to II_1. To confirm this, the IV_1 Jeffery–Hamel solution was used at the inlet with $Re = 45$ and $\alpha = 0.103587$. As expected, the numerical solution moved away from the IV_1 solution downstream from the inlet, the growth did not persist and the solution eventually relaxed to a II_1 Jeffery–Hamel solution far downstream. This can be seen from figure 13 which shows the scaled vorticity $\hat{\zeta}$ on the lower and upper walls of the channel against distance $\hat{X}$, with the IV_1 Jeffery–Hamel flow imposed at $\hat{X} = 0$. Figure 14 shows the streamlines for this flow. A long weak eddy forms on the lower wall, with the streamlines moving towards the upper wall

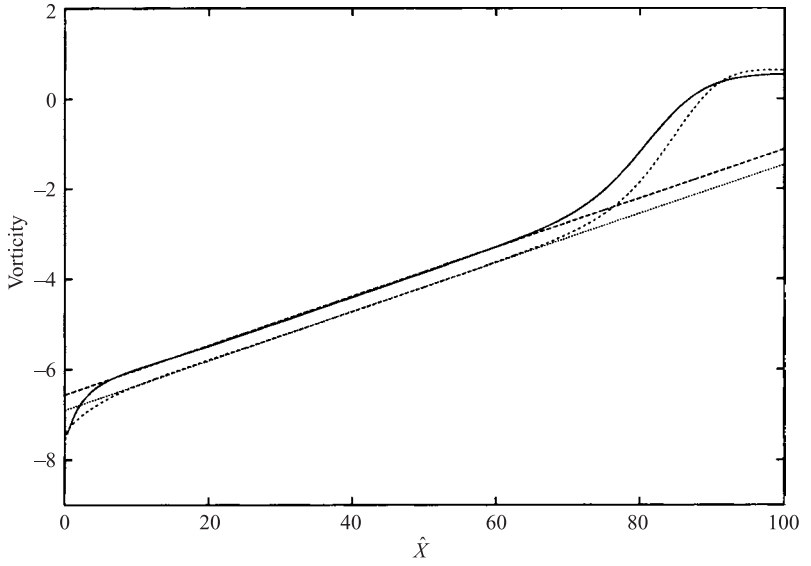

FIGURE 15. The log of the scaled vorticity perturbation ($\log(1-\hat{\zeta}/\hat{\zeta}_{IV})$) against $\hat{X}$ on the walls for $Re=45$, $\alpha=0.103587$, with the IV_1 flow at the inlet. Also shown are straight lines with slope 0.5252α. The lower lines are for the lower wall and the upper lines for the upper wall.

as the region of reverse flow on the upper wall closes. Further downstream, the flow reattaches to the lower wall, and sufficiently far downstream takes the form of the II_1 Jeffery–Hamel flow.

Spatial stability theory (Banks *et al.* 1988) predicts that near the inlet the streamfunction will have the form

$$\psi = \psi_{IV} + r^{\lambda}\psi_1 \ldots \tag{40}$$

where ψ_{IV} is the streamfunction for the IV_1 Jeffery–Hamel flow, $\lambda=0.5252$ is the smallest positive eigenvalue, and ψ_1 the corresponding eigenfunction. It follows that the log of the perturbation to the vorticity in the scaled form (39) should have a linear variation with $\hat{X}$ with slope $\alpha\lambda$. This was found, as can be seen in figure 15. Note that the mismatch near the inlet is due to end effects arising from the fact that the perturbation is zero at the inlet as opposed to the small but finite value implied by (40). Note also that before the solution relaxes to the II_1 state downstream, it passes through a stage in which the flow is nonlinear, although this nonlinearity is not sufficiently strong to generate the change to the upper-branch periodic wave solution which exists at this point in the (Re, α) parameter space.

Another attempt was made to generate the lower branch solution by using a starting condition that periodically flipped between IV_1 and V_1 Jeffery–Hamel solutions with the same wavelength as shown on figure 4 ($\omega=1.498$). Although initially the iteration procedure appeared to be converging on this long-wavelength solution, this tendency was temporary, and the final solution was the upper branch wave.

To summarize, with $\alpha>\alpha_2$ (or equivalently $Re>Re_2=Re(\alpha_2)$) the wave was obtained consistently in a long channel and found to possess the symmetry imposed in (16). For $\alpha_s<\alpha<\alpha_2$ (or $Re_s<Re<Re_2$), whether the extended wave was obtained depended on the conditions at the inlet, and the wave was not found at all for $\alpha<\alpha_s$ (or $Re<Re_s$).

5. Conclusions

In this paper we have argued on the basis of convincing numerical evidence that the wave that Tutty (1996) isolated is born at $\alpha = \alpha_h(Re) < \alpha_2(Re)$ out of a heteroclinic bifurcation across the subcritical pitchfork arms of the Jeffery–Hamel bifurcation at $\alpha = \alpha_2(Re)$. This wave appears initially (spatially) unstable but, as its spatial period decreases with decreasing α (fixed Re), undergoes a saddle-node bifurcation to become stable. Significantly, this stable wave branch extends into $\alpha > \alpha_2(Re)$ so that a realizable solution is predicted by the infinite diverging channel idealization beyond α_2 for the first time. Furthermore, it is clear that the saddle nose never pierces the α-axis ($\alpha_s > 0$) so that this wave has no relevance to plane Poiseuille flow (which corresponds to the limit of $\alpha \to 0$ at fixed Re). In fact, numerical evidence clearly reveals the asymptotic behaviour

$$\frac{\alpha_2 - \alpha_h}{\alpha_2} \sim \frac{13.6}{Re^2} \quad \text{and} \quad \alpha_s \sim \alpha_2 \sim \frac{4.712}{Re} \quad \text{as} \quad Re \to \infty.$$

The importance of these nonlinear waves is largely fundamental, for they are surely one of the many classes of laminar solutions of the Navier–Stokes equations which exist but become unstable as the Reynolds number increases, and ultimately become the repellers in phase space associated with the disorder of turbulent flow. A number of calculations were made using the unsteady version of the Navier–Stokes code (Tutty & Pedley 1993) to investigate, albeit in an unsystematic manner, the temporal response of the steady numerical solutions with an extended channel with a step to a disturbance. For lower Reynolds numbers (e.g. 45 or 125), there was no sign of an instability. However at $Re = 400$, a growing disturbance, much shorter in wavelength than the steady wave, was generated. In this calculation the steady solution was not perturbed, and the unsteady growth was provoked by the remaining small but non-zero residuals in the calculation. The steady flow at this Reynolds number, which is well below that for which all disturbances would decay in a channel with parallel walls, was clearly unstable.

Many experiments on flow in expanding channels do exhibit a train of waves downstream of an expansion which broadly resemble the idealized waves discussed here. In particular, experimental (Sobey 1985) and numerical (Tutty & Pedley 1993) studies of oscillatory flow over a backward-facing step indicate that a vortex wave with the same general appearance is generated during the deceleration phase of the flow. Also, the appearance of the waves considered here, including the double peak in the streamfunction at $Re = 100$, is strongly reminiscent of the wave structure that Rast (1994) found immediately downstream of a collapsible wall section in a two-dimensional channel at $Re = 300$. In this situation, the collapsed section manufactures a sudden expansion and the flow appears to adjust by forming a localized wave form very similar to that found here at $Re = 100$. The one factor which is common to all these flows is that the wave is initiated when the flow is decelerating, either due to modulation of the main stream (Sobey 1985; Tutty & Pedley 1993), or through a change in geometry (Rast 1994 and the current study).

This paper has been concerned mainly with steady two-dimensional waves with a special symmetry. Of course, this is not to exclude the occurrence of other nonlinear wave solutions to the Jeffery–Hamel problem. Indeed, it is natural to conjecture that these waves are only special cases within whole families of generally unsteady, three-dimensional nonlinear waves solutions. Whether the steady two-dimensional waves found here can be used as a stepping stone to reach new solutions in the

Jeffery–Hamel problem or extensions there of (e.g. Stow, Duck & Hewitt 2001; Zaturska & Banks 2003) remains to be seen.

We are grateful to W. H. H. Banks and M. B. Zaturska for sharing their ideas and results on the spatial stability of Jeffery–Hamel flows, to A. R. Champneys and S. R. Wiggins for valuable discussions on heteroclinic bifurcations, and finally to O. E. Jensen for recognising that the waves described here resemble the structures found by M. P. Rast.

REFERENCES

Alleborn, N., Nandakumar, K., Raszillier, H. & Durst, F. 1997 Further contributions on the two-dimensional flow in a sudden expansion. *J. Fluid Mech.* **330**, 169–188.

Banks, W. H. H., Drazin, P. G. & Zaturska, M. B. 1988 On perturbations of Jeffery–Hamel flow. *J. Fluid Mech.* **186**, 559–581.

Batchelor, G. K. 1967 *An Introduction to Fluid Dynamics*. Cambridge University Press.

Cherdron, W., Durst, F. & Whitelaw, J. H. 1978 Asymmetric flows and instabilities in symmetric ducts with sudden expansion. *J. Fluid Mech.* **84**, 13–31.

Ehrenstein. U. & Koch, W. 1991 Three-dimensional wavelike equilibrium states in plane Poiseuille flow. *J. Fluid Mech.* **228**, 111–148.

Fearn, R. M., Mullin, T. & Cliffe, K. A. 1990 Nonlinear flow phenomena in a symmetric sudden expansion. *J. Fluid Mech.* **211**, 595–608.

Fraenkel, L. E. 1962 Laminar flow in symmetrical channels with slightly curved walls. I. On the Jeffery–Hamel solutions for flow between plane walls. *Proc. R. Soc. Lond.* A **267**, 119–138.

Guckenheimer, J. & Holmes, P. 1983 *Nonlinear Oscillations, Dynamical Systems and Bifurcations of Vector Fields*. Springer.

Nakayama, Y. (Ed.) 1988 *Visualised Flow*. Pergamon.

Rast, M. P. 1994 Simultaneous solution of the Navier-Stokes and elastic membrane equations by a finite-element method. *Intl J. Num. Meth. Fluids* **19**, 1115–1135.

Rheinboldt, W. C. & Burkardt, J. V. 1983*a* A locally parametrized continuation process. *ACM Trans. Math. Software* **9**, 215–235.

Rheinboldt, W. C. & Burkardt, J. V. 1983*b* ALGORITHM 596 A program for a locally parameterized continuation process. *ACM Trans. Math. Software* **9**, 236–241.

Sobey, I. J. 1985 Observation of waves during osciallatory channel flow. *J. Fluid Mech.* **151**, 395–426.

Sobey, I. J. & Drazin, P. G. 1986 Bifurcations of two-dimensional channel flows. *J. Fluid Mech.* **171**, 263–287.

Tutty, O. R. 1996 Nonlinear development of flow in channels with non-parallel walls. *J. Fluid Mech.* **326**, 263–284.

Tutty, O. R. & Pedley, T. J. 1993 Oscillatory flow in a stepped channel. *J. Fluid Mech.* **247**, 179–204.

Stow, S. R., Duck, P. W. & Hewitt, R. E. 2001 Three-dimensional extensions to Jeffery-Hamel flow. *Fluid Dyn. Res.* **29**, 25–46.

Zahn, J-P., Toomre, J., Spiegel, E. A. & Gough, D. O. 1974 Nonlinear cellular motions in Poiseuille channel flow. *J. Fluid Mech.* **64**, 319–345.

Zaturska, M. B. & Banks, W. H. H. 2003 Vortex stretching driven by Jeffery-Hamel flow. *Z. Angew. Math. Mech.* **83**, 85–92.